Study of a swirling gas jet emanated from a vortex jet gripper onto a plain barrier

O V Konishcheva, E V Briukhovetskaia, M V Brungardt, A N Shhepin and I V Kudrjavcev

Siberian Federal University 660041 Krasnoyarsk, Russia

maxbrung@gmail.com

Abstract. The interaction of a swirling gas jet emanated from a vortex jet gripper (VJG) onto a plain barrier, and particularly the rarefaction in the gripping area and the impact made by various parameters (compressed air pressure at the inlet, gap size in the contact area) on its value are investigated. The compressed air jet suction force, capable of suspending a flat disc, is determined. The mathematical model determining the picture of jet flow within the system chamber, as well as in the area of contact with the suspended object, is presented.

Introduction

Various industries widely use the vortex systems working on the basis of the swirling gas or liquid jet energy principle [1, 2]. They are especially common in combustion engineering and power technology.

The effect of separating gas into hot and cold streams (Ranque effect), discovered in 1931, is widely used in technology, such as, for example, in vortex refrigerators, in gas and liquid drying and regeneration systems. The ejecting capacity of the vortex flow is widely used in the production of working mixtures in vortex mixers, for transporting various masses from one position to another, for vacuuming working volumes and for separating mixtures into their constituent components. A body placed into a swirling vortex flow acquires a complicated oscillating movement consisting of rotation, rolling with sliding, axial displacement and precessional motion of the body around the vortex tube axis. Thus, a body placed into a vortex tube, performs a searching (orienting) movement around another, motionless body. Moreover, there is a perspective in using vortex chambers for strengthening and cleaning the surface of parts, for applying polish, paint or other coatings.

In classic vortex systems, air is released through the central opening with the smaller diameter than that of the vortex chamber, and herewith, as it is known [3], the tangential component of the velocity in the central part changes under the rigid body rotation rule (v_φ / r = const). At a certain radius r_{max}, the tangential velocity reaches its maximum, and then decreases under the quasipotential flow rule ($v_\varphi r^n$ = const), where n may acquire any values other than one.

Within the radius where $v_\varphi = v_{\varphi\,max}$, the excess pressure equals to zero. The value and the position of the maximum peripheral speed changes depending on the size of the central release opening.

There is a number of works on the experimental and theoretical calculations of $v_{\varphi max}$ and the radius r_{max} where it is located [3, 4, 5, 6]. Vortex systems normally have the optimal release opening

diameter, under which both $v_{\varphi\ max}$ and rarefaction on the axis would be maximal. As this diameter decreases, so do $v_{\varphi\ max}$ and the rarefaction value that reduces to zero; as the opening diameter increases, these values also decrease, but the rarefaction area expands. At that, $v_{\varphi\ max}$ shifts towards the periphery as it decreases.

However, the mentioned works do not consider the situations when a swirling air jet is emanated not through the central opening, but through a small side annular space which happens when the air stream meets a barrier on its way, which may be located at a different distance from the system. In this case, the air jets move not towards the center of the unit, but away from it; it is possible when the opening is expanded towards the chamber outlet. Then the air is emanated through the side annular opening with the height *h,* like in the new construction of VJG suggested herein [7, 8, 9].

Materials and methods

The suggested VJG (figure 1) consists of a cylindrical chamber *1* with the diameter d_k, gradually expanding into the wider end (attachment) *2* with the diameter *D*. In the upper part, there is the case *3*, making up a closed cavity around the chamber for the air supply into the four openings *4* with the diameter d_c.

Under the constant pressure p_U the compressed air is supplied through the opening *5* into the closed cavity around the chamber *3*, and after, going through the tangential openings *4* in the chamber walls and entering the cylindric chamber, it begins to swirl.

In the upper part of the chamber there is an opening that can be either closed with the plug *6*, or a special insert is installed there to narrow the chamber outlet opening and to increase the suction effect of the device. This paper does not consider the latter option.

During the spiral move of the air in the cylindrical chamber *1*, its velocity consists of the three components: radial velocity v_r, tangential velocity v_φ and axial velocity v_z. At that, the radial component v_r is materially less than the tangential v_φ and axial v_z components until the cylindrical chamber gradually expands into its plane surface.

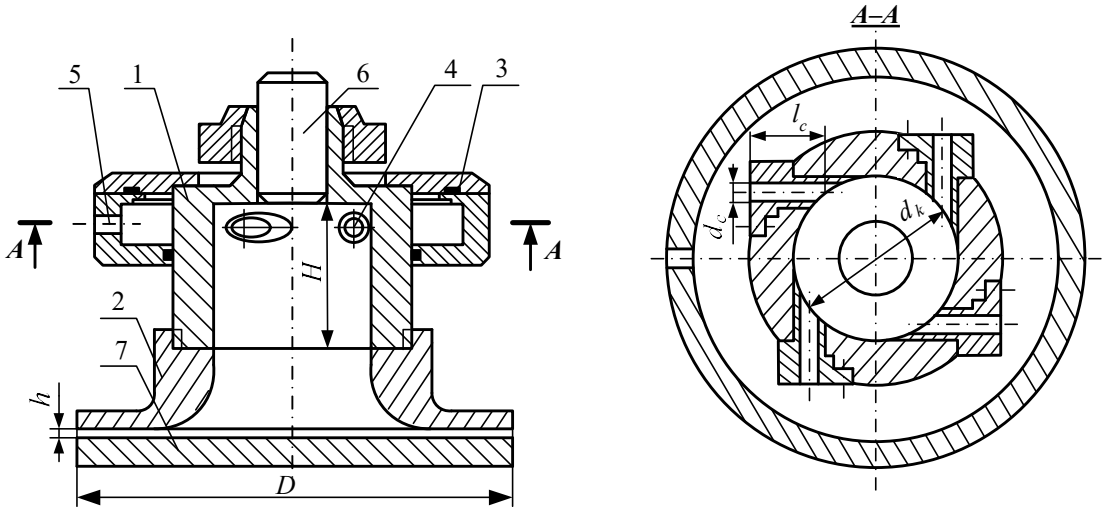

Figure 1. Vortex Jet Gripper

In the bottom part of the system, the radial component v_r becomes comparable to the tangential component v_φ, and the axial component v_z on the opposite becomes irrelevant if a barrier like the plate *7* appears on the way of the air emanated from the chamber.

As the gripper approaches the plate *7* surface*,* the gap *h* between the plane end of the system and the plate decreases, and, as a result, the radial velocity component v_r considerably increases until it finds the greatest value at the chamber outlet to the radial gap. The tangential velocity component v_φ decrease as the distance to the chamber axis increases.

The radial velocity increase effect causes the static pressure drop below the atmosphere pressure, and the greatest rarefaction occurs at a certain value of the gap *h*, the further reduction of which increases the power of the jet that would tend to push the plate 7 away.

If on the VJG end plane there are no stoppers to restrict the movement of the plate 7 along the axis, it begins to oscillate around a certain position, moving towards and away from the plane, finding no efficient working conditions.

The existing VJG structures are based on the well-known suction effect of the jet emanated from a small opening and interacting with the flat, cylindrical or a spherical surface by-passed by it, and the following vortex effect. Under the centrifugal forces produced in a swirling jet, the gas particles shift into the peripheral area of the chamber, forming a spiral vortex jet. In the axis area, the rarefaction zones (recirculation mixing ones) emerge.

A distinctive feature of the interaction between a swirling jet and a flat barrier is the fact that when the barrier is located in close vicinity from the vortex chamber end plane, the excess pressure gets negative.

In this situation, the jet emanated from the cylindrical chamber sticks to the end plane and attracts the barrier. Following the static pressure distribution on the barrier, the total negative force (attraction) exerted upon the barrier exceeds the aggregate positive force (repulsion). Due to this effect, the vortex chamber can be used as a contacted or contactless (depending on the functional requirements) gasostatic suspension.

The emanation of air through the periphery opening facilitates the increased rarefaction due to the radial velocity increase, causing ejection in the central part, and the radial velocity gradient causes the pressure drop, as, if the axial velocity is neglected, then

$$\frac{\mathrm{d}\,p}{\mathrm{d}\,r} = \rho\,\frac{v_\varphi^2}{r} - \rho\,v_r\,\frac{\mathrm{d}\,v_r}{\mathrm{d}\,r} + \mu\,\frac{\mathrm{d}^2 v_r}{\mathrm{d}\,z^2} \tag{1}$$

From this dependence we can see that the pressure decreases more if the radial velocity gradient is positive, i.e. the radial velocity increases farther away from the center. It is possible if at the entry into the annular space v_r equals to the speed of sound; then the further increase in the annular space area causes a velocity increase and a pressure drop, as in de Laval nozzle [10].

In the subsonic flow, the positive gradient of the radial velocity can be also achieved by decreasing the annular space area.

Therefore, the tractive (attractive) force *F*, holding the plate *7,* will appear due to:

− rarefaction in the vortex center;

− rarefaction caused by ejection in the axial area in the high velocity emanation of air into the atmosphere through the opening;

− rarefaction in the plane area due to the considerable increase of the v_r velocity component;

− viscous friction forces.

As it has been mentioned above, the gas flow is relevantly three-dimensional, but moving around the circle all the flow parameters are regularly repeated (after every 90°). For this reason, it is suggested to use a computational mesh being a one quarter of the actual device (figure 2).

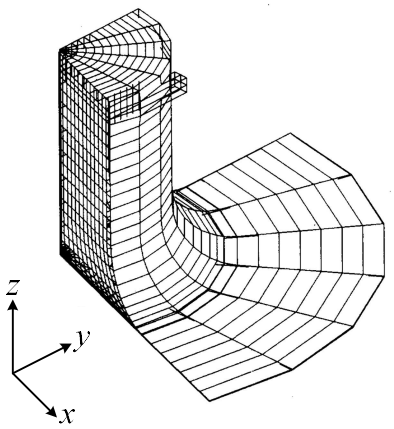

Figure 2. Computational mesh and the cartesian axes

The gas flow inside the system can be considered as established. The orthogonal coordinate system is used. The *z*- axis is oriented along the geometric axis of the system, *x* and *y*-axis go along the plate plane. The sought functions are the tree velocity vector components *u*, *v*, *w*, being velocity vector projects on the coordinate axes *x*, *y, z* correspondingly, and pressure *p*.

For the consideration of turbulence, the so-called $k-\varepsilon$ turbulence model is used [11]. In accordance with this model, two more variables are added to the sought functions: turbulence kinetic energy *k* and turbulence dissipation velocity ε. The gas medium is air with the temperature of 20° C. The presence of any bulk forces is not considered.

In the present problem, the Reynolds number may reach the values of 10^5-10^6, which proves the fact of a turbulent flow.

To calculate the flow in the VJGS, the Reynolds equation is used [12]:

$$\frac{\mathrm{d}\left(\rho \boldsymbol{u}\right)}{\mathrm{d}\,x}+\frac{\mathrm{d}\left(\rho \boldsymbol{v}\right)}{\mathrm{d}\,y}+\frac{\mathrm{d}\left(\rho \boldsymbol{w}\right)}{\mathrm{d}\,z}=0 \tag{2}$$

$$\frac{\mathrm{d}\left(\rho uu\right)}{\mathrm{d}\,x}+\frac{\mathrm{d}\left(\rho uv\right)}{\mathrm{d}\,y}+\frac{\mathrm{d}\left(\rho uw\right)}{\mathrm{d}\,z}=-\frac{\mathrm{d}\,p}{\mathrm{d}\,x}+\frac{\mathrm{d}\,\tau^{\Sigma}_{u\,x}}{\mathrm{d}\,x}+\frac{\mathrm{d}\,\tau^{\Sigma}_{u\,y}}{\mathrm{d}\,y}+\frac{\mathrm{d}\,\tau^{\Sigma}_{u\,z}}{\mathrm{d}\,z} \tag{3}$$

$$\frac{\mathrm{d}\left(\rho vu\right)}{\mathrm{d}\,x}+\frac{\mathrm{d}\left(\rho vv\right)}{\mathrm{d}\,y}+\rho\frac{\mathrm{d}\left(\rho\, vw\right)}{\mathrm{d}\,z}=-\frac{\mathrm{d}\,p}{\mathrm{d}\,y}+\frac{\mathrm{d}\,\tau^{\Sigma}_{vx}}{\mathrm{d}\,x}+\frac{\mathrm{d}\,\tau^{\Sigma}_{vy}}{\mathrm{d}\,y}+\frac{\mathrm{d}\,\tau^{\Sigma}_{vz}}{\mathrm{d}\,z} \tag{4}$$

$$\frac{\mathrm{d}\left(\rho wu\right)}{\mathrm{d}\,x}+\frac{\mathrm{d}\left(\rho wv\right)}{\mathrm{d}\,y}+\frac{\mathrm{d}\left(\rho ww\right)}{\mathrm{d}\,z}=-\frac{\mathrm{d}\,p}{\mathrm{d}\,z}+\frac{\mathrm{d}\,\tau^{\Sigma}_{wx}}{\mathrm{d}\,x}+\frac{\mathrm{d}\,\tau^{\Sigma}_{wy}}{\mathrm{d}\,y}+\frac{\mathrm{d}\,\tau^{\Sigma}_{wz}}{\mathrm{d}\,z}, \tag{5}$$

$$\tau^{\Sigma}_{ij}=\tau_{ij}\ +\tau^{t}_{ij} \tag{6}$$

$$\tau^{t}_{ij}=-\rho\,\boldsymbol{u}'_i\,\boldsymbol{u}'_j, \tag{7}$$

where ρ is air density, τ_{ij} is viscous stress, $\rho u'_i u'_j$ is turbulent stress, τ^{t}_{ij} – is turbulent momentum flux, $i, j = 1, 2, 3$ for the convenience in equations (6) and (7) $u_1 \equiv u$, $u_2 \equiv v$, $u_3 \equiv w$, $x_1 \equiv x$, $x_2 \equiv y$, $x_3 \equiv z$ are accepted. For example, $\tau_{12} \equiv \tau_{uy}$.

Viscous stresses are calculated with the proportions:

$$\tau_{ii} = 2\mu \frac{\mathrm{d}\boldsymbol{u}_i}{\mathrm{d}x_i};$$
$$\tau_{ij} = \mu\left(\frac{\mathrm{d}\boldsymbol{u}_i}{\mathrm{d}x_j} + \frac{\mathrm{d}\boldsymbol{u}_j}{\mathrm{d}x_i}\right), \tag{8}$$

where μ is dynamic air viscosity under normal conditions.

The turbulent momentum fluxes are usually presented as a product of gradients of the corresponding mean values and the effective turbulent transfer rate:

$$\tau_{ij}^{t} = \mu_{eff}\left(\frac{\mathrm{d}\boldsymbol{u}_i}{\mathrm{d}\,x_j} + \frac{\mathrm{d}\,\boldsymbol{u}_j}{\mathrm{d}\,x_i}\right) - \frac{2}{3}\delta_{ij}\rho k, \tag{9}$$

where μ_{eff} is the effective turbulent viscosity, k is kinetic turbulence energy, $\delta_{ij} = 0$, if $i \neq j$, $\delta_{ij} = 1$, if $i = j$.

Effective turbulent viscosity is expressed as follows:

$$\mu_{eff} = \mu + C_\mu \rho \frac{k^2}{\varepsilon}, \tag{10}$$

where μ is the dynamic viscosity factor, k is kinetic turbulence energy, ε is kinetic energy dissipation velocity, C_μ is an empirical constant.

The equation determining the turbulence kinetic energy and its dissipation velocity for the standard $k-\varepsilon$ model look as follows:

$$\frac{\mathrm{d}\left(\rho\, uk\right)}{\mathrm{d}\,x} + \frac{\mathrm{d}\left(\rho v k\right)}{\mathrm{d}\,y} + \frac{\mathrm{d}\left(\rho v k\right)}{\mathrm{d}\,z} = \frac{\mathrm{d}}{\mathrm{d}\,x}\left(\frac{\mu_{eff}}{\sigma_k}\frac{\mathrm{d}\,k}{\mathrm{d}\,x}\right) + \\ + \frac{\mathrm{d}}{\mathrm{d}\,y}\left(\frac{\mu_{eff}}{\sigma_k}\frac{\mathrm{d}\,k}{\mathrm{d}\,y}\right) + \frac{\mathrm{d}}{\mathrm{d}\,z}\left(\frac{\mu_{eff}}{\sigma_k}\frac{\mathrm{d}\,k}{\mathrm{d}\,z}\right) + G - \rho\varepsilon \tag{10}$$

$$\frac{\mathrm{d}\left(\rho\, u\varepsilon\right)}{\mathrm{d}\,x} + \frac{\mathrm{d}\left(\rho v\varepsilon\right)}{\mathrm{d}\,y} + \frac{\mathrm{d}\left(\rho w\varepsilon\right)}{\mathrm{d}\,z} = \frac{\mathrm{d}}{\mathrm{d}\,x}\left(\frac{\mu_{eff}}{\sigma_\varepsilon}\frac{\mathrm{d}\varepsilon}{\mathrm{d}\,x}\right) + \frac{\mathrm{d}}{\mathrm{d}\,y}\left(\frac{\mu_{eff}}{\sigma_\varepsilon}\frac{\mathrm{d}\varepsilon}{\mathrm{d}\,y}\right) + \\ + \frac{\mathrm{d}}{\mathrm{d}\,z}\left(\frac{\mu_{eff}}{\sigma_\varepsilon}\frac{\mathrm{d}\varepsilon}{\mathrm{d}\,z}\right) + C_1\frac{\varepsilon}{k}G - C_2\rho\frac{\varepsilon^2}{k} + C_3\frac{G^2}{\rho k} \tag{11}$$

The empirical constants $C_\mu = 0.09$, $\sigma_k = 1.0$, $\sigma_\varepsilon = 1.3$, $C_1 = 1.43$, $C_2 = 1.92$, $C_3 = 0$ for the standard $k-\varepsilon$ model were adopted from Launder (Launder, Spalding, 1974), for the modified Chen-Kim $k-\varepsilon$ model [13] $\sigma_k = 0.8$, $\sigma_\varepsilon = 1.15$. $C_1 = 1.15$, $C_2 = 1.9$, $C_3 = 0.25$.

Turbulent generation velocity G equals

$$G = \sum_{i,j=1}^{3} \tau_{ij}\frac{\mathrm{d}\,u_j}{\mathrm{d}\,x_j} \tag{12}$$

Results and discussion

The device used in the present research (figure 1) had a chamber with the diameter $d_k = 70$ mm, the nozzle diameter $d_c = 4$ mm, the nozzle length $l_c = 55$ mm, the chamber height $H = 40$ mm and the attachment diameter $D = 200$ mm. The gap h varied from 0.1 mm to 2.5 mm.

The compressed air pressure at the VJG inlet was varied from 0.2 at to 3 at. At that, Q consumption changed from 8.5 m^3/h to 26.5 m^3/h.

The computation revealed that the standard k–ε turbulence model does not consistently consider the swirling jet peculiarities, since it causes material deviations from the experimental data. The results closer to the experimental ones are provided by the modified Chen k–ε model.

Figures 3-8 show only some examples of the results obtained both theoretically and experimentally. Figure 3 and 4 demonstrate the patterns of air movement velocities in the horizontal cross-sections of the gap between the bottom surface of the device and the plane of plate 7. The distance z from the plate to the considered cross-section and the dimension of the gap h are indicated in the figure legend.

In figure 3 we can see that in the cylindrical part of the device the quasi-rigid spinning zone is formed, where the tangential velocity value is increased in direct proportion to the radius. Further down the stream, in the chamber expansion area, the linear profile of the quasi-rigid spinning becomes parabolic (figure 4) with the maximum shifted from the wall towards the axis.

The results demonstrate that the radial velocity component is small. In the gap area (figure 5) there is an increase in the radial velocity component, which continues increasing the farther it gets from the axis.

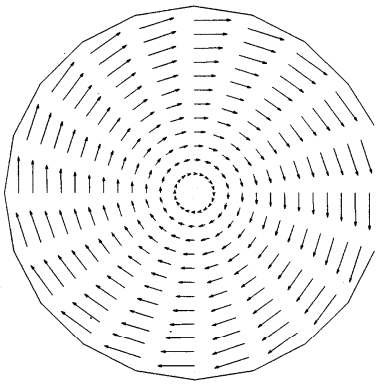

Figure 3. Velocity profile in the cross-section z = 45.8 mm, h = 0.6 mm

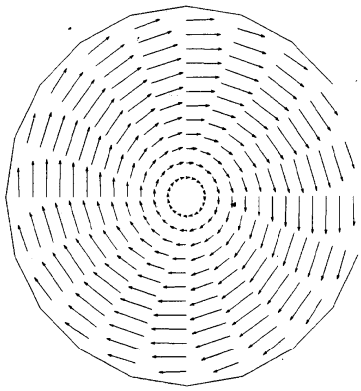

Figure 4. Velocity profile in the cross-section z = 12.75 mm, h = 0.6 mm

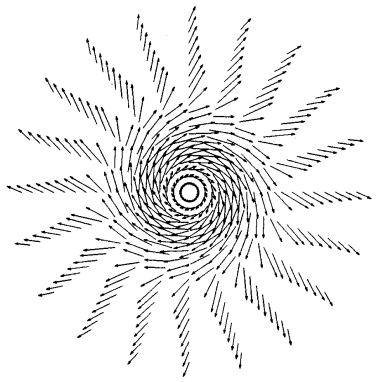

Figure 5. Velocity profile in the cross-section z = 0.45 mm, h = 0.6 mm.

Figure 6 presents the diagrams of dependence of the pressure in the gap area from the radius r at different values of the gap h. The consumption was 21 m^3/h.

As the gap increases, the rarefaction around the central axis is growing. With the further increase to h = 2 mm, an insignificant drop in the rarefaction is observed, but the curve gets straighter with no leaps in the area where $r \approx 0.5$ mm.

At smaller gaps in the area, the leap increases; the excess pressure is present, which causes the repulsion of the plate. With such gaps, the tractive force of the system is less.

Figure 7 presents the changes in the pressure difference caused by the radius at the gap h = 0.6 mm. The dots represent the experimental values, the pecked line shows the calculation with the standard k–ε model, the solid line indicates the calculation with the modified Chen model.

It is worth noticing that both models brought the results close to the experimental ones: they correctly forecast the location of extreme values and create closely similar lines. We can see that the modified model is closer to the experiment.

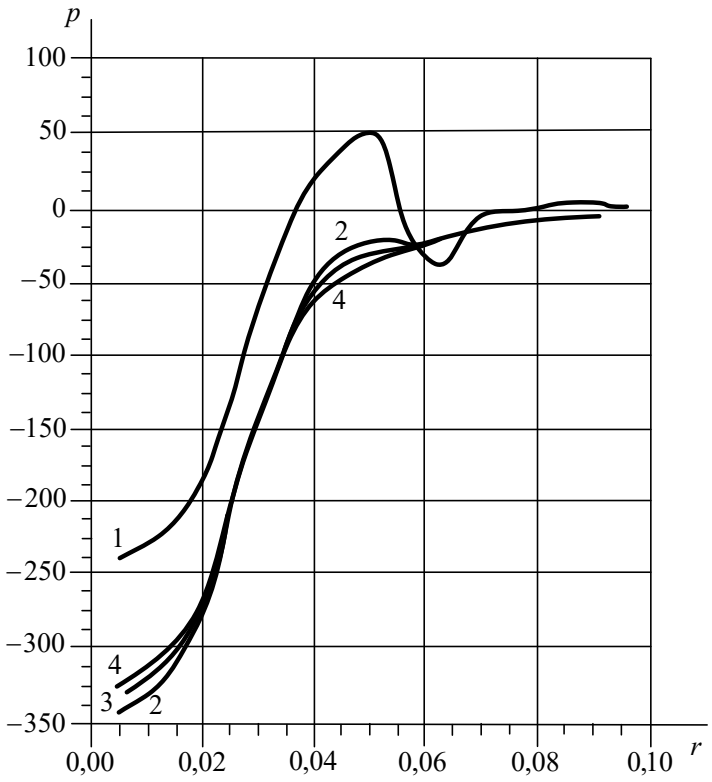

Figure 6. Dependence of the pressure difference (mm H_2O) from the radius (m) under different gap h (mm): 1 – 0.6; 2 – 1.2; 3 – 1.5; 4 – 2.0.

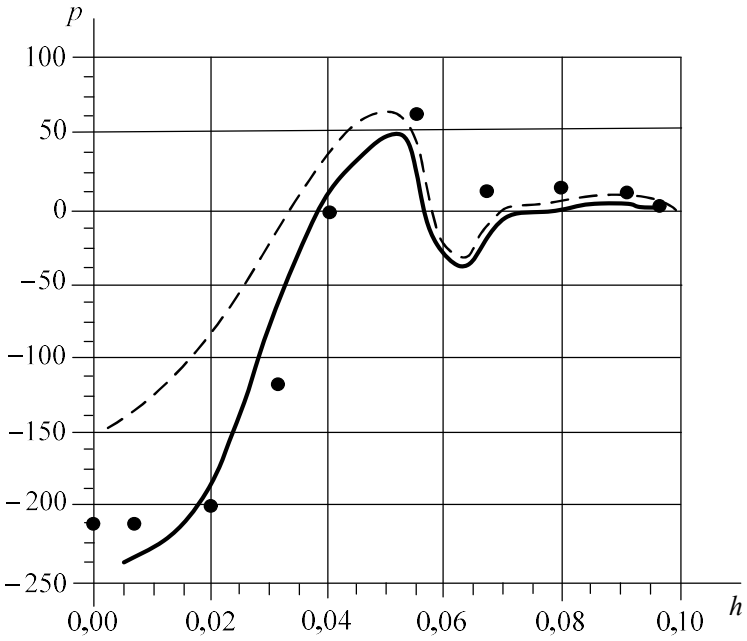

Figure 7. Dependence of the pressure difference (mm H_2O) from radius (m) under the h = 0.6 mm
(● – experiment; solid line – Chen model, pecked line – standard k – ε model)

Conclusion

The research results show that the tractive (retention) force increases as per the parabolic law as the compressed air pressure (consumption) increases, and it directly depends on the geometric parameters, for instance, of the gap *h*. The effect of other parameters is negligible and was not considered herein.

Thus, under certain gap dimensions the rarefaction, and, consequently, the traction force reach the maximum values. It allows to install stoppers on the bottom surface of the device to hold the object in the optimal distance.

The greatest tractive force of the device under the inlet pressure 2.8 at and the consumption 29.4 m^3/h constituted 96 N, and in this case the suspended disc with the weight did not contact with the device, i.e. the gap was voluntarily set.

The obtained result may be improved by installing the stoppers; then the disc would stick to them and would not be able to get close enough for the repulsion forces to emerge. A special insert intended to increase the radial velocity at the entry of the annual space (gap) would considerably increase the rarefaction and the traction force.

Therefore, the performed experimental and theoretical research of the vortex jet grippers proved that they can be successfully used for gripping and transporting various objects.

Reference

[1] Krasov V B 1981 *Vikhrevoy potok v avtomatizatsii tekhnologicheskikh protsessov Int: Technological processes automatization* pp 93-104

[2] Merkulov A P 1997 *Vikhrevoy potok i ego primenenie v tekhnike* (Moscow, Mashinostroenie) p 185

[3] Gol'dshtik M A 1981 *Vikhrevye potoki*.(Novosibirsk, Nauka) p 365

[4] Volchkov E P, Dvornikov, N A, Terekhov V I 1986 *Zhurnal prikladnoy mekhaniki i tekhnicheskoy fiziki* vol 4 pp 59-68

[5] Pirolishvili Sh A, Poliaev V M, Sergeev, M.N 2000 *Vikhrevoy effekt. Eksperiment, teoriia, tekhnicheskie resheniia*.(Moscow, UNPTs Energomash) p 412

[6] Chernysh N K 2010 *Teoriia i raschet ideal'nykh vikhrevykh ustrotstv*.(Moscow, Medisont) p 370

[7] Konishcheva O V, Konishchev V M 1998 *Vakuumnoe gruzozakhvatnoe ustroystvo*. Patent 2114782 // BI. 1998. № 19

[8] Konishcheva O V, Sinenko E G, Briukhovetskaia E V 2012 *Tekhnologiia mashinostroeniia*. 11 pp 22-24

[9] Konishcheva O V, Briukhovetskaia E V, 2012. *Sovremennye tekhnologii. Sistemny analiz. Modelirovanie* 4 pp 57-60

[10] Landau L D, Lifschitz E M 1988 *Gidrodinamika* (Moscow, Nauka) p 203

[11] Launder B E, Spalding D B 1974 Comput. Methods Appl. Mech. & Eng. 1 (3) pp 269-289.

[12] Loytsiansky L G 1987 *Liquid and gas mechanics* (Moscow, Nauka) p 365

[13] Chen Y S 1988 AIAA pp 88-0417.